Effect of pressure on the thermal cracking and polymerization of pentacosane (n-C_{25}), an n-alkane

*Ayako Shinozaki**

Faculty of Science, Hokkaido University, N10 W8, Kita-ku, Sapporo, Hokkaido 060-0810, Japan

* Corresponding author

E-mail: shinozaki.aya@sci.hokudai.ac.jp

Keywords: hydrocarbon, amorphous carbon, high pressure, pyrolysis, subduction zone, carbon cycle

Abstract

Hydrocarbons are important carbon components in the subducting slab and that play a crucial role in the Earth's deep carbon cycle. In this study, the thermal reaction of pentacosane (n-C_{25}), a long n-alkane, was experimentally investigated under high-pressure and high-temperature conditions at 0.5–1.5 GPa and 360–400 °C. The gas chromatography–mass spectrometry (GC/MS) analyses of the reaction products revealed that the radical reaction of n-C_{25} proceeded above 360 °C at 0.5 GPa and above 380 °C at 1.5 GPa, while the rate constant decreased with increasing pressure. Lighter n-alkanes and heavier straight/branched alkanes were detected in the reaction products. The formation of lighter n-alkanes indicates thermal cracking progression, even at high-pressure conditions. During thermal cracking, lighter 1-alkenes were likely to form, but were instead rapidly added to the initial n-C_{25} to form heavier alkanes when enhanced by pressure. Thus, lighter 1-alkenes were not detected in the reaction products. As the secondary reaction, the heavier alkanes were polymerized with dehydrogenation to form amorphous carbon when the remaining percentage of the initial material became <10 % and <20 % at 0.5 and 1.5 GPa, respectively, while the lighter n-alkanes were detected simultaneously. Both lighter alkanes with high H/C ratios and amorphous carbon with a low H/C ratio eventually formed through the reaction of n-alkanes at high-pressure and high-temperature conditions of the deep Earth.

27 **Table of Contents graphic**

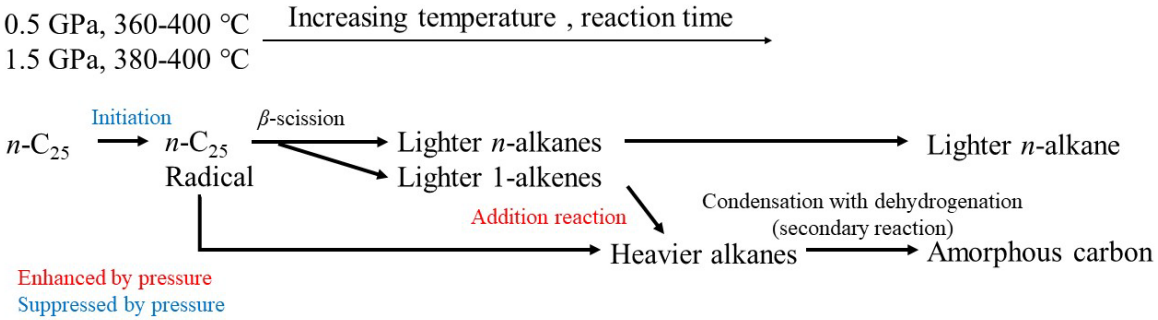

28

29

Introduction

The stability and chemical reactions of hydrocarbons are crucial in Earth and planetary science because of their widespread occurrence, including the interstellar medium[1, 2], carbonaceous meteorites[3, 4], and organic sediments at the Earth's surface[5]. Furthermore, hydrocarbons were found in the mantle peridotite xenoliths[6]. Organic sediments including hydrocarbons are likely to be supplied from the Earth's surface to the deep Earth with subducting slabs[7, 8]. In addition, abiotic hydrocarbons are synthesized in the deep Earth by Fischer–Tropsch reactions[9], and by the reduction of carbonates[10, 11]. Stability and chemical reactions of hydrocarbons in the deep Earth are essential for understanding the deep carbon cycles of the Earth, but are currently poorly understood. In the Earth's interior, both temperature and pressure increase with increasing depth. Generally, high temperature would enhance thermal cracking with the production of lighter molecules, whereas high pressure would induce polymerization with the formation of heavier compounds[12-17]. Thus, the chemical reactions of hydrocarbons at high-pressure and high-temperature (HPHT) conditions are expected to be complicated and are the subjects of ongoing debate.

Methane, the simplest hydrocarbon, is an important component in C-O-H fluids in the Earth's mantle[18], and its chemical reactions under HPHT conditions have been widely investigated. The formation of ethane and heavier hydrocarbons with the dehydrogenation and polymerization of

methane progressed above 1,000 K, comparable to the HPHT conditions of Earth's upper mantle and the interiors of icy planets[19-23]. The reaction advanced significantly with increasing temperature and eventually formed graphitic carbon/diamond above 3000 K. Thermodynamic calculations and theoretical studies have pointed out that alkanes heavier than methane become more stable with increasing pressure and temperature[24, 25], but much less is known on the chemical reactions of heavier alkanes under HPHT conditions. Chemical reactions of propane (C_3H_8) progressed partially at temperatures of approximately 1000 K and pressures of 3–22 GPa to form both heavier alkanes, such as butane (C_4H_{10}), pentane (C_5H_{12}), and hexane (C_6H_{14}), and lighter hydrocarbons such as methane, suggesting that C-C bond formation and cleavage of C-C and C-H bonds occurred simultaneously[26]. The formation of hydrogenated amorphous carbon from *n*-hexane at ~20 GPa and 1000 K, as well as diamond formation from longer *n*-alkanes (C_8H_{18} to $C_{19}C_{40}$) above 3000 K at 10–20 GPa were reported[27, 28]. Theoretical and experimental studies have suggested that when the unbranched alkane chains reach some critical length, the chains assume a folded conformation rather than a linear one[29, 30]. Pressure-induced transition from linear to fold molecular conformations was observed in longer *n*-alkanes (C_7H_{16}, $C_{18}H_{38}$, and $C_{23}H_{48}$), where the reaction pressure decreased as the carbon numbers of *n*-alkanes increased[31-33]. Kinks in fold structures are likely to facilitate cracking of the longer chains, hence, reactions in longer alkanes exposed to high temperatures after compression may be the result

64 of individual processes on the alkane chain length, and it is necessary to investigate the reaction
65 individually. [32, 33]

66 Thermal reactions of *n*-alkanes at lower pressure conditions, such as those of the shallow
67 crust, have been investigated with significant attention in the field of petrochemistry. The complex
68 reaction products were quantitatively and quantitatively evaluated by using gas chromatography–
69 mass spectrometry (GC/MS) analyses. Free-radical reaction pathways are considered to be the
70 dominant reaction pathways of alkanes[34-36]. The series of reactions is initiated by the cleavage of C-
71 C bonding, followed by H-transfer to form radicals of the initial alkane. Lighter *n*-alkanes and 1-
72 alkenes are formed by beta-scissions from the radicals of the initial alkane. Furthermore, heavier
73 straight and branched alkanes are formed by addition reactions between the initial alkane and the 1-
74 alkenes. The effect of pressure on the thermal reactions was also investigated previously[37-39], however,
75 the pressure ranges of most of these studies were limited to below ~100 MPa.

76 In this study, the thermal reaction of a long straight alkane, pentacosane (*n*-C_{25}), was
77 investigated experimentally at 0.5 and 1.5 GPa in a closed system. Pentacosane was selected as a
78 model hydrocarbon compound due to its occurrence in various environments, including petroleum
79 crudes[40], ultramafic hydrothermal field on the Mid-Atlantic Ridge[41], and carbonaceous meteorites[1, 3].
80 In addition, *n*-C_{25} was found in tectonites and mantle xenoliths[6] thus, its presence in the deep Earth

has been suggested. Investigating the stability and reactions of *n*-C_{25} under HPHT conditions are essential for determining its origin, as well as its role in the deep carbon cycle. The complex reaction products were identified and evaluated analytically using GC/MS to reveal the reaction mechanisms and the effect of pressure.

Experimental methods

Pentacosane ($C_{25}H_{52}$, Tokyo Chemical Industry Co. LTD., purity >99.0 %) and aluminum oxide (Al_2O_3, FUJIFILM Wako Pure Chemical Corporation) were used as the initial materials for the HPHT experiments. Aluminum oxide was powdered and cleaned with acetone, then heated in an oven at 450 °C for 4 h to remove organic contaminants. Pentacosane and aluminum oxide were mixed in an agate mortar with a weight ratio approximately 1:4. A gold sample capsule with a 4 mm outer diameter was cleaned with dichloromethane and heated in an oven at 450 °C for 4 h to remove organic contaminants prior to encapsulating the sample. Approximately 15 mg of the initial material was filled into the gold capsule and welded. The capsule was pressurized using a tungsten carbide piston-cylinder type apparatus equipped with a hydraulic press. A cylinder with a 4 mm inner diameter was used without a pressure medium. Sealing plates made of stemless seats and copper/phosphor bronze (0.2 mm thick) were placed at the top and bottom of the sample capsule. The sample was first compressed to the target pressure at room temperature, and then heated using a band-type external

heater surrounding the cylinder. The temperature was measured using a K-type thermocouple attached to the top of the cylinder. The detail of the apparatus was described in a previous study[42].

The samples after the HPHT experiments were recovered from the capsules in distilled dichloromethane solvent by drilling to prevent the reaction products from escaping. The solution was initially filtered by a membrane filter to extract the soluble products from the insoluble products. For the soluble products, mass spectrometry was performed using a GC/MS (Agilent 6890/5973N) equipped with a 30 m × 0.25 mm I.D. capillary column, with a 0.25 μm layer of stationary phase (DB-5HT, Agilent Technology Co.). The representative GC column temperature program was as follows; maintained at 45 °C for 3 min, then increased from 45 to 325 °C at a rate of 3 °C/min, and then finally held at 325 °C for 10 min. Helium was used as the carrier gas (1 mL/min). An *m*/*z* scan range from 50 to 550 was used. Methyl laurate ($C_{13}H_{26}O_2$) and methyl stearate ($C_{19}H_{38}O_2$) were used as internal standards for the quantitative analyses. Raman spectra of the insoluble products were measured using micro-Raman spectrometry. The applied Raman spectrometer was equipped with a semiconductor laser (λ = 532 nm) with approximately 5.5 mW output power on the sample surface, an optical microscope with an objective lens, a single polychromator, and a CCD-detector. Scattered light was dispersed using a grating with 1,200 grooves/mm. The Raman bands of naphthalene and neon emission lines were used for Raman shift calibration. The spectral resolution was approximately

115 1 cm^{-1}. To check that laser irradiation did not damage the samples, the spectra were measured
116 repeatedly at the same points. Changes in the Raman spectra due to laser damage were not observed.
117 The appearance of the samples was also checked before and after laser irradiation using an optical
118 microscope; there were no considerable changes observed.

119 **Results**

120 The HPHT experiments with *n*-C_{25} performed at 0.5 and 1.5 GPa and at temperatures ranging from
121 360 to 400 °C are listed in Table 1. Figure 1a and b represents logarithmic plots of the remaining *n*-
122 C_{25} at 0.5 and 1.5 GPa, respectively. A remarkable decrease in *n*-C_{25} was observed at 360-400 °C, 0.5
123 GPa and at 380-400 °C, 1.5 GPa, while the reaction was not observed from the samples at 360 °C,
124 1.5 GPa (runs 15 and 16). The remaining ratio of the starting material decreased with both increasing
125 reaction time and temperature. The reaction times and the logarithms of the remaining ratios show a
126 linear relationship, indicating that the reaction is a first-order reaction. Table 2 presents the calculated
127 rate constants for *n*-C_{25} at 0.5 GPa (360–400 °C) and 1.5 GPa (380–400 °C), indicating that the
128 reaction rate decreases with increasing pressure.

129

130

131 **Table 1** Experimental Conditions of the Present Study

Run no.	Pressure (GPa)	Temperature (°C)	Reaction time (h)	Remaining n-C_{25} (%)
1	0.5	360	48	91.7
2	0.5	360	96	77.2
3	0.5	360	192	47.8
4	0.5	370	48	91.3
5	0.5	370	96	71.0
6	0.5	370	192	26.5
7	0.5	380	24	77.0
8	0.5	380	48	56.7
9	0.5	380	96	27.6
10	0.5	400	8	68.3
11	0.5	400	24	25.7
12	0.5	400	48	8.55
13	0.5	400	48	1.2
14	0.5	400	96	0.4
15	1.5	360	48	100.2
16	1.5	360	96	101.2
17	1.5	380	48	92.7
18	1.5	380	96	82.1
19	1.5	380	192	68.3
20	1.5	400	48	83.8
21	1.5	400	96	27.0
22	1.5	400	96	17.4
23	1.5	400	192	4.6
24	1.5	400	192	1.6

132

133 **Table 2** Rate Constants Obtained for the n-C_{25} reaction

	0.5 GPa	1.5 GPa
360 °C	1.11×10^{-6}	
370 °C	1.99×10^{-6}	
380 °C	3.75×10^{-6}	5.33×10^{-7}
400 °C	1.68×10^{-5}	5.63×10^{-6}

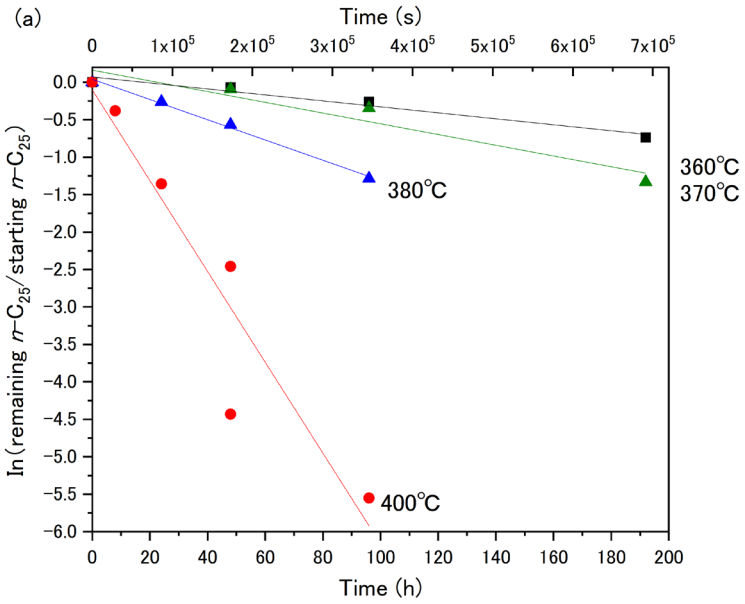

134

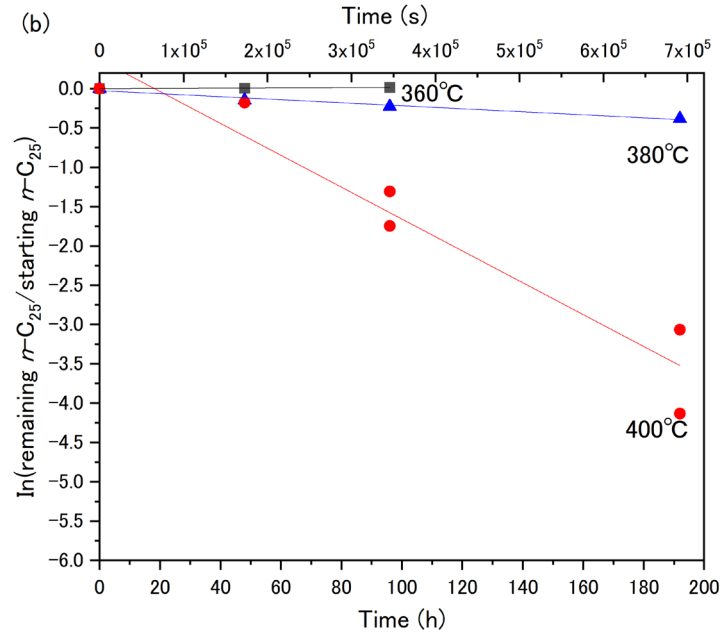

135

136 **Figure 1** Remaining ratio of *n*-C_{25} between 360 and 400 °C at (a) 0.5 and (b) 1.5 GPa.

Figure 2 shows a representative total ion chromatogram (TIC) of the reaction products recovered from 0.5 GPa and 400 °C for 24 h (run 11). Many intense peaks were detected with almost equal intervals at shorter retention times than that from *n*-C_{25}. The peaks were identified as lighter *n*-alkanes (*n*-C_9 to *n*-C_{24}) by their retention times and the mass spectra. Although *n*-C_{23} and *n*-C_{24} were contained in the initial material, as well as *n*-C_{26} and *n*-C_{27}, the amounts of these contaminants were significantly lower than those detected in the reaction products (Table S1). In the slightly shorter retention times than that of *n*-C_{25}, the peaks assignable as C_{25} alkenes were detected, which had $[M]^{\bullet+}$ = 350 in their mass spectra (Figure S1a), while peaks from alkenes with carbon numbers < 24 were not detected in the reaction products. Many peaks were detected at longer retention times than that from *n*-C_{25}, suggesting the formation of heavier hydrocarbons. Most of the heavier reaction products had fragmental peaks of m/z = 57, indicating that the reaction products were alkanes, some of which were identified as the longer straight alkanes (*n*-C_{26} to *n*-C_{32}). An intense fragmented peak of m/z = 351 was found from most of the other heavier products (Figure S1b–d), which is considered as a fragmented peak of $C_{25}H_{51}^{\bullet+}$. The results suggest that most of the heavier reaction products were branched alkanes formed by an addition reaction between *n*-C_{25} and alkyl fractions.

153

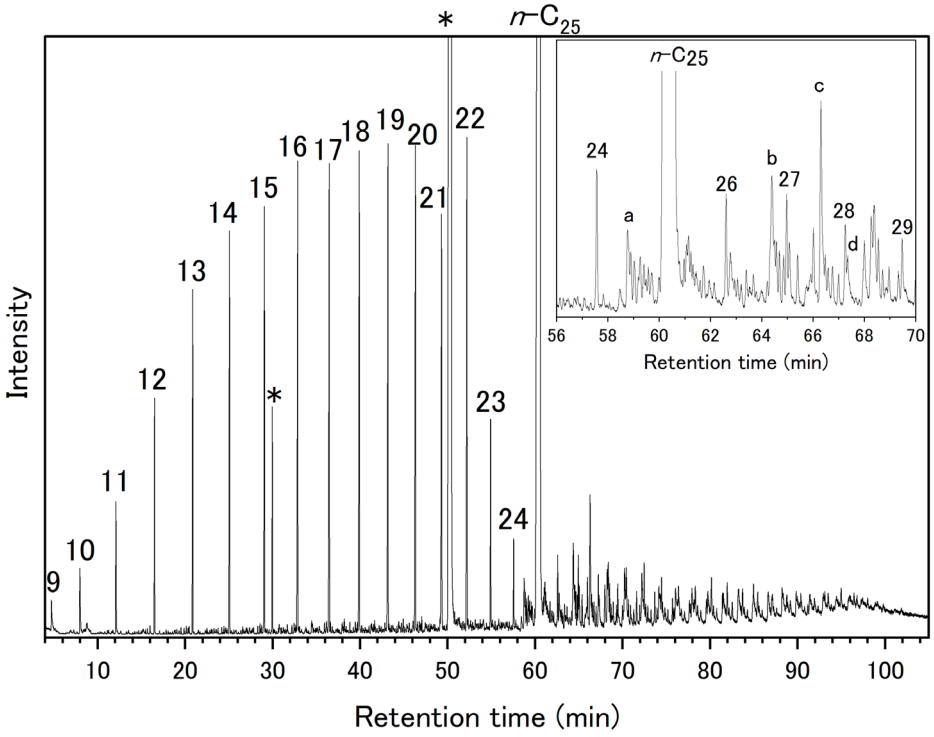

154

155 **Figure 2** Representative TIC of GC/MS measurements from the reaction product of the sample at 0.5 GPa

156 and 400 °C for 24 h (run 11). Numbers 9–27 represent *n*-alkane peaks. Asterisk represents the internal

157 standard peak. Inset is an enlarged view at 57–70 min. The mass spectra of peaks a–d are represented in

158 Figure S1.

159

160 Figure 3a shows representative molar yields of lighter *n*-alkanes from *n*-C_9 to *n*-C_{24} at 0.5 GPa and

161 400 °C with different reaction times. The molar yields of the lighter *n*-alkanes increased with

increasing carbon numbers up to *n*-C_{22} after reaction times of 8 h (Figure 3a, Table S1). The yields of *n*-C_{23} and n-C_{24} were significantly lower than those of the other lighter *n*-alkanes. It is indicated that C-C bond cracking did not likely occur at the end of the chain, but rather in the interior C-C bonds as reported during the thermal cracking of *n*-C_{25} at lower pressure conditions[39]. After the reactions at 48 and 96 h, the molar yields show an opposite trend, namely the molar yields decreased with decreasing the carbon numbers from *n*-C_{22} to around *n*-C_{10}. At 1.5 GPa, a similar trend of the molar yields of lighter *n*-alkanes was observed (Figure 3b). Namely, molar yields of the lighter *n*-alkanes increased with increasing carbon numbers up to *n*-C_{22} after the reaction for 48 h, while the molar yields decreased with decreasing carbon numbers from *n*-C_{22} to around *n*-C_9 after the reaction for 96 and 192h. The sum of the molar yields of the lighter *n*-alkanes between *n*-C_9 and *n*-C_{24} shows an increasing trend with the decrease of the remaining *n*-C_{25}, and the total molar yields reached around 11 % and 15 % at 0.5 GPa (run 13) and 1.5 GPa (run 21), respectively (Table S1).

(a)

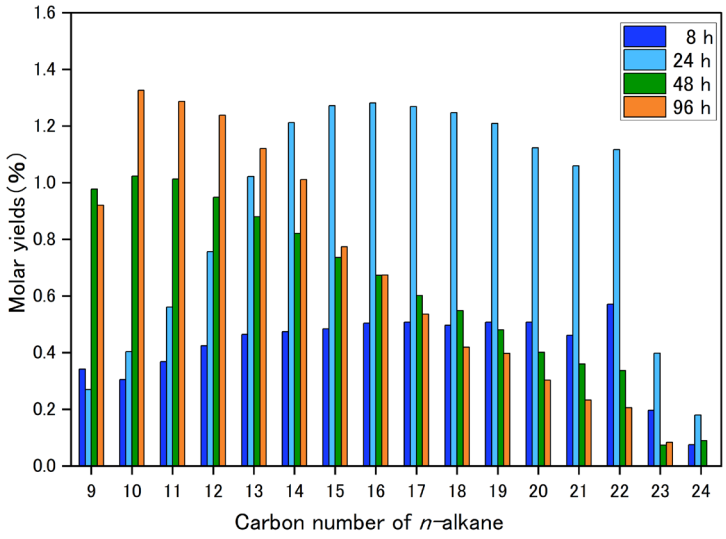

(b)

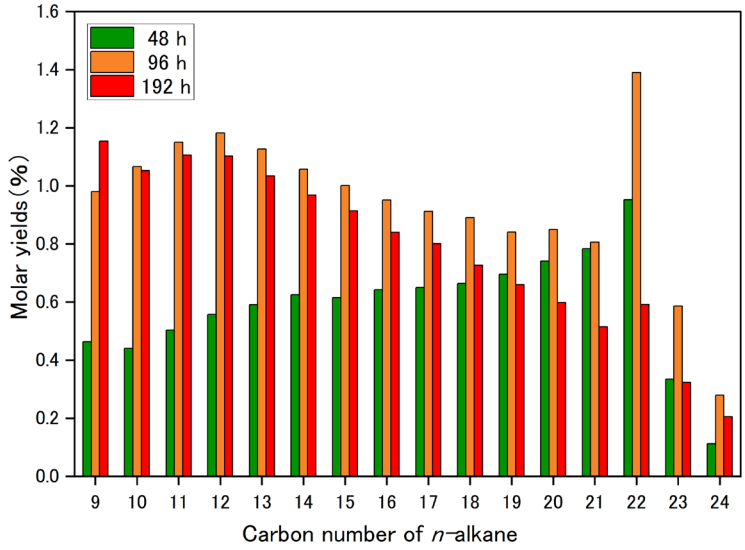

Figure 3 Molar yields of the lighter *n*-alkanes at (a) 0.5 GPa and 400 °C and (b) 1.5 GPa and 400 °C with changing reaction times. The yields are an average of two runs with the same experimental conditions for 48 h (runs 12 and 13) at 0.5 GPa and for 96 h (runs 21 and 22) and 192 h (runs 23 and 24) at 1.5 GPa.

Figure 4a shows representative single ion chromatograms of m/z = 57 at 0.5 GPa, 400 °C with different reaction times from 8 to 96 h. Many heavier and lighter alkane peaks were observed from the samples after heating for 8 and 24 h, for which the remaining percentages of the starting material were 68.3 % and 25.7 % (runs 10 and 11), respectively. The relative intensity of the peaks from the heavier alkanes decreased and almost disappeared after heating for 48 and 96 h, where the remaining percentages of the initial material were 1.2 % and 0.4 %, respectively (runs 13 and 14), while the light *n*-alkanes still remained. The total yield of the heavier alkanes was 7.8 wt.% after heating for 24 h (run 11) and decreased significantly to <1 wt.% after heating for 48 and 96 h (runs 12–14, respectively) as listed in Table S2. The extracted solutions from runs 12–14 changed to a yellow color, while the solution of the other recovered samples and the starting material were transparent. It is implying the formation of some soluble heavier conjugated organics in runs 12–14, but the organics were not able to be analyzed using the GC/MS analysis applied in this study. For the single ion chromatogram of the reaction products at 1.5 GPa and 400 °C, as shown in Figure 4b, the peaks from the heavier alkanes were still observed, but the total yields decreased from 5.9 to ~2 wt%, while the remaining percentage of the initial material decreased from 17.4 % to <5 % with reaction times increased from 96 to 192 h (Table S2). The total yield of the reaction products did not reach 100%, suggesting that the lighter *n*-alkanes less than C_8 and the heavier molecules might be formed

196 by thermal cracking and addition reactions, but those products were not able to be detected by the

197 GC/MS analysis applied herein.

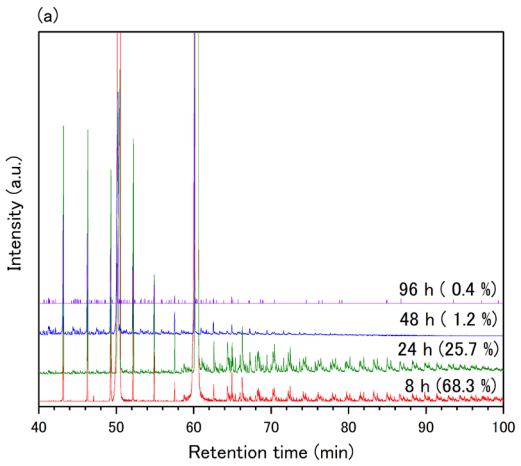

198

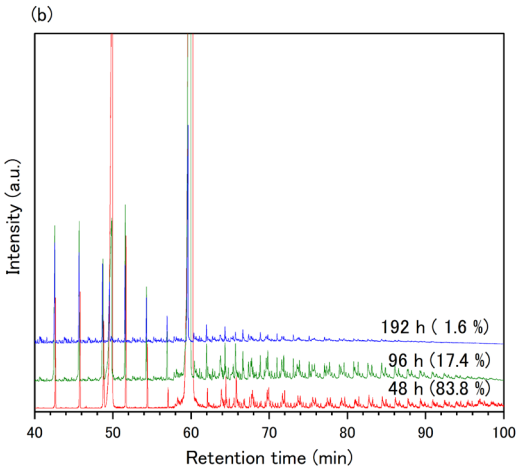

199

200 **Figure 4** Single ion chromatograms (*m/z* = 57) at (a) 0.5 GPa and 400 °C and at (b) 1.5 GPa and 400 °C

201 for different reaction times. The intensities of the chromatograms were normalized by the peak intensity

202 of methyl laurate, the internal standard. The remaining percentages of *n*-C_{25} are shown in brackets.

203

Insoluble carbonaceous materials with aluminum oxide were obtained from the samples after heating to 400 °C at 0.5 GPa for >48 h, and to 400 °C at 1.5 GPa, for >96 h (runs 13, 14, and 22–24). Figure 5a and b show the representative Raman spectra of the insoluble materials obtained from the sample at 0.5 GPa and 400 °C for 96 h (run 14) and from the sample at 1.5 GPa, and 400 °C for 192 h (run 24), respectively. Peaks were observed at 1254, 1331, 1487, and 1604 cm^{-1} (run 14) (the fitting details are shown in Figure S2a and Table S3a), which were assignable as the D4, D1, D3, and G_L bands of carbonaceous material[43, 44]. The G_L band consisted of G and D2 bands, but could not be separated. The second-order bands were observed at around 2500–3200 cm^{-1}, but were not well-resolved. The peak frequencies and shapes were similar to those of soot[43] and amorphous carbon[45], rather than amorphous hydrogenated carbon[46]. In the case of amorphous hydrogenated carbon, which contains >20 % hydrogen, the peak intensity of the G band is much higher than that of the D band, in contrast to that observed from the insoluble material of the present study. The intensities of D_1/G_L in runs 14 and 24 samples were 0.73 and 0.70, respectively, suggesting low sp^3/sp^2 ratios[45]. The spectra obtained from the insoluble material at 0.5 GPa showed rises in the baseline, which were hardly observed at 1.5 GPa. The rises in the baseline suggest that the insoluble material contained some fluorescent substances such as conjugated organics. Similar Raman spectra of amorphous carbon

were obtained from the reaction products of *n*-hexane and cyclohexane after the DAC experiments of 20 GPa and 1000 K[28], and from the reactants of the shocked compression of benzene[47].

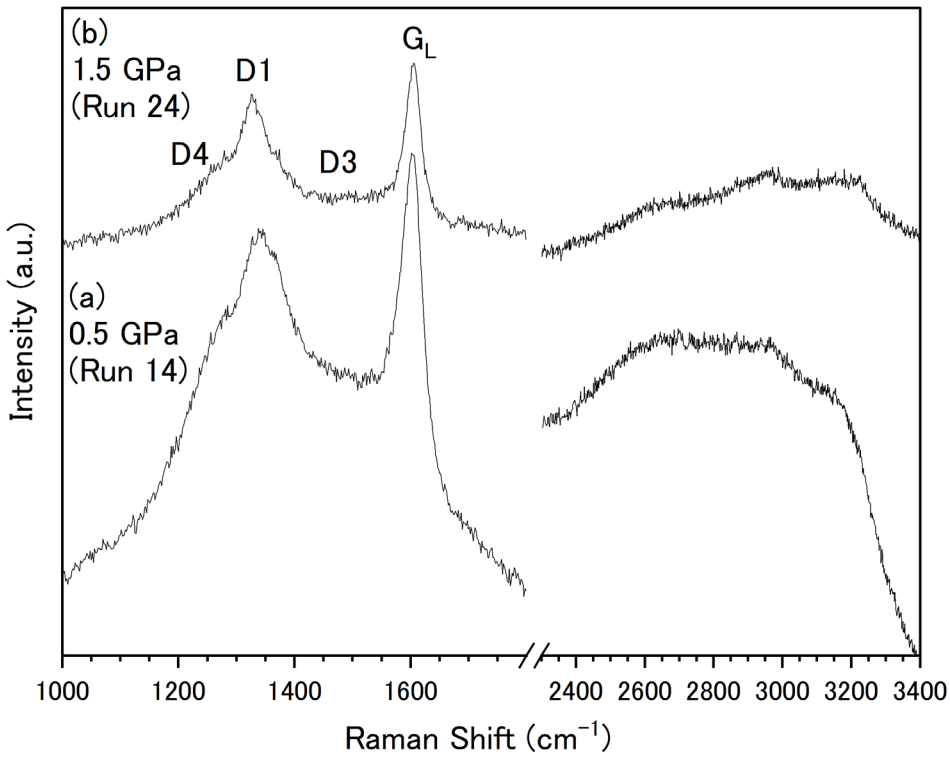

Figure 5 Representative Raman spectra for the insoluble products of (a) 0.5 GPa and 400 °C for 96 h (run 14) and at (b) 1.5 GPa and 400 °C for 192 h (run 24).

Discussion

The thermal reaction of *n*-C_{25} progressed with increasing temperature >360 °C at 0.5 GPa and >380 °C at 1.5 GPa. The reaction also progressed with increasing reaction time and followed the first-order

229 fraction. Both lighter *n*-alkanes and heavier straight/branched alkanes formed via the reaction. These
230 experimental results indicate that the free-radical thermal reaction progressed under high-pressure
231 conditions at 0.5 and 1.5 GPa. The reaction rate of *n*-C_{25} at 1.5 GPa was significantly smaller than
232 that at 0.5 GPa at the same temperature, indicating that initiation of the reaction was suppressed with
233 increasing pressures. The reaction rate of the *n*-alkanes increased with increasing pressure up to ~40
234 MPa, above which it decreased with increasing pressure[39, 48, 49]. Similar reaction rate changes with
235 pressure have been reported for *n*-C_{25} at 12–80 MPa [39]. The reaction rate at 350 °C increased from 7.4
236 × 10^{-7} s^{-1} to 12.3 × 10^{-7} s^{-1} at 12 MPa and 40 MPa, respectively. Then, the reaction rate decreased with
237 increasing pressure. The reaction rate constant for *n*-C_{25} at 80 MPa was 8.6 × 10^{-7} s^{-1}, which was
238 almost consistent with that at 12 MPa. The reaction rates at 400 °C were 3.75×10^{-6} s^{-1} and 1.68×10^{-5}
239 s^{-1} at 0.5 GPa and 1.5 GPa, respectively (Table 1), which were considerably smaller than that at 12
240 MPa, (4.3× 10^{-5} s^{-1})[39]. The results suggest that the decreasing reaction rate of *n*-C_{25} with increasing
241 pressure occurred continuously up to at least 1.5 GPa.
242 The thermal reactions of *n*-alkanes formed lighter 1-alkenes by beta scission, as well as
243 lighter *n*-alkanes[34-36], although 1-alkenes with < C_{24} were not detected in the reaction products, even
244 in the low conversion rate both at 0.5 and 1.5 GPa. It is in contrast to that observed in the radical
245 reactions of *n*-alkanes at lower pressures at around 10 MPa, in which both lighter *n*-alkanes and 1-

246 alkenes were formed from thermal cracking and were obtained in almost the same degree[37, 50]. Heavier
247 straight and branched alkanes were detected in this study and were likely to be formed by the addition
248 reaction of 1-alkenes and *n*-C_{25}. It is suggested that lighter 1-alkenes were formed by beta-scission of
249 *n*-C_{25} with *n*-alkanes at first. Then, the lighter 1-alkenes rapidly reacted with *n*-C_{25} to form various
250 heavier alkanes at 0.5 and 1.5 GPa. Consequently, the radical addition reaction would prefer to
251 progress under higher pressure conditions. Similar pressure dependence for the formation of heavier
252 alkanes was reported in the case of radical reactions of *n*-hexane and *n*-hexadecane ($C_{16}H_{34}$)[37, 51].
253 Polymerization is a common reaction in hydrocarbons under high pressure, especially in the case of
254 unsaturated hydrocarbons, in which the double carbon bonds reacted to form a single bond by addition
255 reaction, reported as the pressure-induced polymerization of ethylene and propene[52, 53]. Aromatic
256 compounds were not detected by the GC/MS analysis in this study. However, C_{14+} aromatics were
257 detected from the reaction products of *n*-C_{25} at 12 MPa[39]. Polymerization of aromatic compounds,
258 such as benzene and naphthalene with formation of sp^3 bonding was induced by compression up to
259 <20 GPa, even at room temperature[54, 55]. However, no chemical reactions of *n*-hexane and
260 cyclohexane were detected at least up to 40 GPa at room temperature[28]. It is possible that unsaturated
261 aromatic compounds became less stable at high pressures compared with saturated hydrocarbons and
262 therefore were less likely to form by the thermal reaction of *n*-alkanes with increasing pressure. While

gold capsules were often used in the experiments on hydrocarbon reactions[39, 49, 56], it should be noted that catalytic effect of metals on hydrocarbon reactions under HPHT conditions was theoretically predicted[25]. Further studies are necessary to verify the catalytic effect of gold capsules on hydrocarbon reactions.

Amorphous carbon was formed as the product of secondary reactions when the remainder of the initial *n*-C_{25} dropped below ~10 and ~20 % at 0.5 and 1.5 GPa, respectively. In the same recovered samples, considerable decreases in the heavier straight and branched alkanes were observed in the GC/MS analyses. These results suggest that condensation with dehydrogenation of heavier alkanes progressed to form amorphous carbon. At 12 MPa, the formation of insoluble carbonaceous products, so-called cokes, by the reaction of *n*-C_{25} was reported when the remaining *n*-C_{25} dropped below 6 %[39]. Insoluble amorphous carbon was obtained when the remaining percentage of the starting material dropped below ~10 and ~20 % at 0.5 and 1.5 GPa, respectively; namely, the secondary reaction initiated even at lower reaction rates with increasing pressure. The secondary reaction with condensation and dehydrogenation would prefer to progress under higher pressure conditions. The lighter *n*-alkanes were still detected with the formation of amorphous carbon, suggesting that both amorphous carbon with a low H/C ratio and lighter *n*-alkanes with higher H/C ratios were formed via the thermal reaction of *n*-alkanes.

Conclusions

The effect of pressure on the thermal reaction of a long *n*-alkane, pentacosane (*n*-C_{25}) was investigated by using GC/MS analyses of the reaction products recovered from 0.5 and 1.5 GPa and between 360 and 400 °C. Radical reactions of *n*-C_{25} progressed at HPHT conditions >360 °C, 0.5 GPa and >380 °C, 1.5 GPa, while the rate constants of the reaction decreased with increasing pressure. The lighter *n*-alkanes of *n*-C_9 to *n*-C_{24} and heavier straight/branched alkanes were obtained from the reaction products, while lighter 1-alkenes were not detected even though they were considered to be formed by beta scission. At the high pressures, 1-alkenes were quickly added to the *n*-C_{25} to form the heavier alkanes, so 1-alkenes were not detected in the reaction products. The addition reaction of unsaturated carbons was shown to proceed preferentially with increasing pressure. The heavier alkanes were polymerized with dehydrogenation as a secondary reaction, eventually forming amorphous carbon at 0.5 GPa, 400 °C >48 h and at 1.5 GPa, 400 °C, >96 h when the remaining starting *n*-C_{25} reduced to <10 % and <20 %, respectively. The HPHT experimental conditions of the present study are comparable to the geotherm of cold subducting slabs up to around 50 km in depth[57]. The experimental results demonstrate that radical beta scission of long *n*-alkanes occurs even under HPHT conditions of the deep Earth. Both lighter alkanes with high H/C ratios and amorphous carbon with a low H/C ratio are likely to form eventually from the reaction of *n*-alkanes.

Supporting Information

Representative mass patterns of C_{25} alkene and heavier branched alkanes, fitting results of the Raman spectra for the insoluble products, tables of molar yields of shorter *n*-alkanes, and total yields of the heavier alkanes (PDF).

Funding Sources

This work was supported by JSPS KAKENHI (Nos. 19K1480809 and 22K03769). This work was partly supported by a grant for Basic Science Research Projects from The Sumitomo Foundation, (No. 200403).

Acknowledgements

I would like to thank Ms. K. Takimoto and Dr. K. Mimura for constructive discussions on this research. I am grateful to Professor N. Suzuki for his helpful advice on the GC/MS analyses.

References

(1) Ehrenfreund, P.; Charnley, S. B. Organic molecules in the interstellar medium, comets, and meteorites: A voyage from dark clouds to the early earth. *Annual Review of Astronomy and Astrophysics* **2000**, *38*, 427-483. DOI: 10.1146/annurev.astro.38.1.427.

(2) Pendleton, Y. J.; Allamandola, L. J. The organic refractory material in the diffuse interstellar medium: Mid-infrared spectroscopic constraints. *Astrophysical Journal Supplement Series* **2002**, *138* (1), 75-98. DOI: 10.1086/322999.

(3) Cronin, J. R.; Pizzarello, S. Aliphatic-hydrocarbons of the murchison meteorite *Geochimica et Cosmochimica Acta* **1990**, *54* (10), 2859-2868. DOI: 10.1016/0016-7037(90)90020-l.

(4) Kissin, Y. V. Hydrocarbon components in carbonaceous meteorites. *Geochimica et Cosmochimica Acta* **2003**, *67* (9), 1723-1735. DOI: 10.1016/s0016-7037(02)00982-1.

(5) Behar, F.; Vandenbroucke, M. Chemical modeling of kerogens. *Organic Geochemistry* **1987**, *11* (1), 15-24. DOI: 10.1016/0146-6380(87)90047-7.

(6) Sugisaki, R.; Mimura, K. Mantle hydrocarbons -abiotic or biotic. *Geochimica et Cosmochimica Acta* **1994**, *58* (11), 2527-2542. DOI: 10.1016/0016-7037(94)90029-9.

(7) Clift, P. D. A revised budget for Cenozoic sedimentary carbon subduction. *Reviews of Geophysics* **2017**, *55* (1), 97-125. DOI: 10.1002/2016rg000531.

(8) Plank, T.; Manning, C. E. Subducting carbon. *Nature* **2019**, *574* (7778), 343-352. DOI: 10.1038/s41586-019-1643-z.

(9) Sephton, M. A.; Hazen, R. M. On the Origins of Deep Hydrocarbons. In *Carbon in Earth*, Hazen, R. M., Jones, A. P., Baross, J. A. Eds.; Reviews in Mineralogy & Geochemistry, Vol. 75; 2013; pp 449-465.

(10) Mukhina, E.; Kolesnikov, A.; Kutcherov, V. The lower pT limit of deep hydrocarbon synthesis by $CaCO_3$ aqueous reduction. *Scientific Reports* **2017**, *7*, 5749. DOI: 10.1038/s41598-017-06155-6.

(11) Tao, R. B.; Zhang, L. F.; Tian, M.; Zhu, J. J.; Liu, X.; Liu, J. Z.; Hofer, H. E.; Stagno, V.; Fei, Y. W. Formation of abiotic hydrocarbon from reduction of carbonate in subduction zones: Constraints from petrological observation and experimental simulation. *Geochimica Et Cosmochimica Acta* **2018**, *239*, 390-408. DOI: 10.1016/j.gca.2018.08.008.

(12) Depeyre, D.; Flicoteaux, C.; Chardaire, C. Pure n-hexadecane thermal steam cracking. *Industrial & Engineering Chemistry Process Design and Development* **1985**, *24* (4), 1251-1258. DOI: 10.1021/i200031a059.

(13) Aribike, D. S.; Susu, A. A. Kinetics and mechanism of the thermal cracking of *n*-heptane. *Thermochimica Acta* **1988**, *127*, 247-258. DOI: 10.1016/0040-6031(88)87501-4.

(14) Behar, F.; Vandenbroucke, M.; Teermann, S. C.; Hatcher, P. G.; Leblond, C.; Lerat, O. Experimental simulation of gas generation from coals and a marine kerogen. *Chemical Geology* **1995**, *126* (3-4), 247-260. DOI: 10.1016/0009-2541(95)00121-2.

(15) Wang, Q. D.; Wang, J. B.; Li, J. Q.; Tan, N. X.; Li, X. Y. Reactive molecular dynamics simulation and chemical kinetic modeling of pyrolysis and combustion of n-dodecane. *Combustion and Flame* **2011**, *158* (2), 217-226. DOI: 10.1016/j.combustflame.2010.08.010.

(16) Fitzgibbons, T. C.; Guthrie, M.; Xu, E. S.; Crespi, V. H.; Davidowski, S. K.; Cody, G. D.; Alem, N.; Badding, J. V. Benzene-derived carbon nanothreads. *Nature Materials* **2015**, *14* (1), 43-47. DOI: 10.1038/nmat4088.

(17) Naumoya, A. S.; Lepeshkin, S. V.; Oganov, A. R. Hydrocarbons under Pressure: Phase Diagrams and Surprising New Compounds in the C-H System. *Journal of Physical Chemistry C* **2019**, *123* (33), 20497-20501. DOI: 10.1021/acs.jpcc.9b01353.

(18) Frost, D. J.; McCammon, C. A. The redox state of Earth's mantle. *Annual Review of Earth and Planetary Sciences* **2008**, *36*, 389-420. DOI: 10.1146/annurev.earth.36.031207.124322.

(19) Benedetti, L. R.; Nguyen, J. H.; Caldwell, W. A.; Liu, H. J.; Kruger, M.; Jeanloz, R. Dissociation of CH_4 at high pressures and temperatures: Diamond formation in giant planet interiors? *Science* **1999**, *286* (5437), 100-102. DOI: 10.1126/science.286.5437.100.

(20) Hirai, H.; Konagai, K.; Kawamura, T.; Yamamoto, Y.; Yagi, T. Polymerization and diamond formation from melting methane and their implications in ice layer of giant planets. *Physics of the Earth and Planetary Interiors* **2009**, *174* (1-4), 242-246. DOI: 10.1016/j.pepi.2008.06.011.

(21) Kolesnikov, A.; Kutcherov, V. G.; Goncharov, A. F. Methane-derived hydrocarbons produced under upper-mantle conditions. *Nature Geoscience* **2009**, *2* (8), 566-570. DOI: 10.1038/ngeo591.

(22) Lobanov, S. S.; Chen, P. N.; Chen, X. J.; Zha, C. S.; Litasov, K. D.; Mao, H. K.; Goncharov, A. F. Carbon precipitation from heavy hydrocarbon fluid in deep planetary interiors. *Nature Communications* **2013**, *4*, 3446. DOI: 10.1038/ncomms3446.

(23) Serovaiskii, A.; Kutcherov, V. Formation of complex hydrocarbon systems from methane at the upper mantle thermobaric conditions. *Scientific Reports* **2020**, *10* (1), 4559. DOI: 10.1038/s41598-020-61644-5.

(24) Kenney, J. F.; Kutcherov, V. A.; Bendeliani, N. A.; Alekseev, V. A. The evolution of multicomponeint systems at high pressures: VI. The thermodynamic stability of the hydrogen-carbon system: The genesis of hydrocarbons and the origin of petroleum. *Proceedings of the National Academy of Sciences of the United States of America* **2002**, *99* (17), 10976-10981. DOI: 10.1073/pnas.172376899.

(25) Spanu, L.; Donadio, D.; Hohl, D.; Schwegler, E.; Galli, G. Stability of hydrocarbons at deep Earth pressures and temperatures. *Proceedings of the National Academy of Sciences of the United States of America* **2011**, *108* (17), 6843-6846. DOI: 10.1073/pnas.1014804108.

(26) Kudryavtsev, D. A.; Fedotenko, T. M.; Koemets, E. G.; Khandarkhaeva, S. E.; Kutcherov, V. G.; Dubrovinsky, L. S. Raman Spectroscopy Study on Chemical Transformations of Propane at High Temperatures and High Pressures. *Scientific Reports* **2020**, *10* (1), 1483. DOI: 10.1038/s41598-020-58520-7.

(27) Zerr, A.; Serghiou, G.; Boehler, R.; Ross, M. Decomposition of alkanes at high pressures and temperatures. *High Pressure Research* **2006**, *26* (1), 23-32. DOI: 10.1080/08957950600608931.

(28) Yang, X.; Li, Y. P.; Wang, Y. J.; Zheng, H. Y.; Li, K.; Mao, H. K. Chemical transformations of *n*-hexane and cyclohexane under the upper mantle conditions. *Geoscience Frontiers* **2021**, *12* (2), 1010-1017. DOI: 10.1016/j.gsf.2020.06.006.

(29) Luttschwager, N. O. B.; Wassermann, T. N.; Mata, R. A.; Suhm, M. A. The Last Globally Stable Extended Alkane. *Angewandte Chemie-International Edition* **2013**, *52* (1), 463-466. DOI: 10.1002/anie.201202894.

(30) Byrd, J. N.; Bartlett, R. J.; Montgomery, J. A. At What Chain Length Do Unbranched Alkanes Prefer Folded Conformations? *Journal of Physical Chemistry A* **2014**, *118* (9), 1706-1712. DOI: 10.1021/jp4121854.

(31) Basu, A.; Murphy, P.; Mookherjee, M.; Haberl, B.; Boehler, R. High-pressure behavior of a linear chain alkane, tricosane. *Journal of Applied Physics* **2020**, *127* (10). DOI: 10.1063/1.5143450.

(32) Basu, A.; Mookherjee, M.; Schiffert, C.; Haberl, B.; Boehler, R. Spectroscopic Investigation of the High-Pressure Behavior of Aliphatic Hydrocarbon: Implications for Planetary Processes. *Acs Earth and Space Chemistry* **2021**, *5* (3), 449-456. DOI: 10.1021/acsearthspacechem.0c00259.

(33) Basu, A.; Mookherjee, M.; McMahan, E.; Haberl, B.; Boehler, R. Behavior of Long-Chain Hydrocarbons at High Pressures and Temperatures. *Journal of Physical Chemistry B* **2022**, *126* (13), 2530-2537. DOI: 10.1021/acs.jpcb.1c10786.

(34) Rice, F. O.; Herzfeld, K. F. The thermal decomposition of organic compounds from the standpoint of free radicals VI The mechanism of some chain reactions. *Journal of the American Chemical Society* **1934**, *56*, 284-289. DOI: 10.1021/ja01317a006.

(35) Kossiakoff, A.; Rice, F. O. Thermal decomposition of hydrocarbons, resonance stabilization and isomerization of free radicals. *Journal of the American Chemical Society* **1943**, *65*, 590-595. DOI: 10.1021/ja01244a028.

(36) Ford, T. J. Liquid-phase thermal decomposition of hexadecane -reaction mechanisms. *Industrial & Engineering Chemistry Fundamentals* **1986**, *25* (2), 240-243. DOI: 10.1021/i100022a010.

(37) Khorasheh, F.; Gray, M. R. High-pressure thermal cracking of *n*-hexadecane. *Industrial & Engineering Chemistry Research* **1993**, *32* (9), 1853-1863. DOI: 10.1021/ie00021a008.

(38) Jackson, K. J.; Burnham, A. K.; Braun, R. L.; Knauss, K. G. Temperature and pressure dependence of *n*-hexadecane cracking. *Organic Geochemistry* **1995**, *23* (10), 941-953. DOI: 10.1016/0146-6380(95)00068-2.

(39) Behar, F.; Vandenbroucke, M. Experimental determination of the rate constants of the *n*-C_{25} thermal cracking at 120, 400, and 800 bar: Implications for high-pressure/high-temperature prospects. *Energy & Fuels* **1996**, *10* (4), 932-940. DOI: 10.1021/ef9600366.

(40) Kissin, Y. V. Cataganesis and composition of pertoroleum -origin of *n*-alkanes and isoalkanes in pertoroleumcrudes *Geochimica et Cosmochimica Acta* **1987**, *51* (9), 2445-2457. DOI: 10.1016/0016-7037(87)90296-1.

(41) Holm, N. G.; Charlou, J. L. Initial indications of abiotic formation of hydrocarbons in the Rainbow ultramafic hydrothermal system, Mid-Atlantic Ridge. *Earth and Planetary Science Letters* **2001**, *191* (1-2), 1-8. DOI: 10.1016/s0012-821x(01)00397-1.

(42) Shinozaki, A.; Mimura, K.; Nishida, T. Decomposition and oligomerization of 2,3-naphthyridine under high- pressure and high-temperature conditions. *Scientific Reports* **2019**, *9*, 7335. DOI: 10.1038/s41598-019-43868-2.

(43) Sadezky, A.; Muckenhuber, H.; Grothe, H.; Niessner, R.; Poschl, U. Raman micro spectroscopy of soot and related carbonaceous materials: Spectral analysis and structural information. *Carbon* **2005**, *43* (8), 1731-1742. DOI: 10.1016/j.carbon.2005.02.018.

(44) Kouketsu, Y.; Mizukami, T.; Mori, H.; Endo, S.; Aoya, M.; Hara, H.; Nakamura, D.; Wallis, S. A new approach to develop the Raman carbonaceous material geothermometer for low-grade metamorphism using peak width. *Island Arc* **2014**, *23* (1), 33-50. DOI: 10.1111/iar.12057.

(45) Ferrari, A. C.; Robertson, J. Interpretation of Raman spectra of disordered and amorphous carbon. *Phys. Rev. B* **2000**, *61* (20), 14095-14107. DOI: 10.1103/PhysRevB.61.14095.

(46) Casiraghi, C.; Ferrari, A. C.; Robertson, J. Raman spectroscopy of hydrogenated amorphous carbons. *Phys. Rev. B* **2005**, *72* (8), 1-14. DOI: 10.1103/PhysRevB.72.085401.

(47) Mimura, K.; Nishida, T. Hydrogen and Hydrocarbon Gases, Polycyclic Aromatic Hydrocarbons, and Amorphous Carbon Produced by Multiple Shock Compression of Liquid Benzene up to 27.4 GPa. *Journal of Physical Chemistry A* **2017**, *121* (34), 6471-6480. DOI: 10.1021/acs.jpca.7b06627.

(48) Fabuss, B. M.; Smith, J. O. Thermal Cracking of Pure Saturated Hydrocarbons. In *Advances in petroleum chemistry and refining*, Vol. 9; 1964; pp 156-201.

(49) Bounaceur, R.; Lannuzel, F.; Michels, R.; Scacchi, G.; Marquaire, P. M.; Burkle-Vitzthum, V. Influence of pressure (100 Pa-100 MPa) on the pyrolysis of an alkane at moderate temperature (603 K-723 K): Experiments and kinetic modeling. *Journal of Analytical and Applied Pyrolysis* **2016**, *122*, 442-451. DOI: 10.1016/j.jaap.2016.10.022.

(50) Fabuss, B. M.; Borsanyi, A. S.; Satterfield, C. N.; Lait, R. I.; Smith, J. O. Rapid thermal cracking of *n*-hexadecane at evaluated pressures *Industrial & Engineering Chemistry Process Design and Development* **1962**, *1* (4), 293-299. DOI: 10.1021/i260004a011.

(51) Domine, F. Kinetics of hexane pyrolysis at very high-pressures.1.1 experimental study *Energy & Fuels* **1989**, *3* (1), 89-96. DOI: 10.1021/ef00013a016.

(52) Chelazzi, D.; Ceppatelli, M.; Santoro, M.; Bini, R.; Schettino, V. Pressure-induced polymerization in solid ethylene. *Journal of Physical Chemistry B* **2005**, *109* (46), 21658-21663. DOI: 10.1021/jp0536495.

(53) Citroni, M.; Ceppatelli, M.; Bini, R.; Schettino, V. High-pressure reactivity of propene. *J. Chem. Phys.* **2005**, *123* (19), 194510. DOI: 10.1063/1.2109947.

(54) Ciabini, L.; Santoro, M.; Bini, R.; Schettino, V. High pressure reactivity of solid benzene probed by infrared spectroscopy. *J. Chem. Phys.* **2002**, *116* (7), 2928-2935. DOI: 10.1063/1.1435570.

(55) Shinozaki, A.; Nagai, T.; Kagi, H.; Nakano, S. Pressure-induced irreversible amorphization of naphthalene and nitrogen-containing heteroaromatic compounds at room temperature. *Chem. Phys. Lett.* **2020**, *739*, 6, Article. DOI: 10.1016/j.cplett.2019.136921.

(56) Sokol, A. G.; Tomilenko, A. A.; Bul'bak, T. A.; Sokol, I. A.; Persikov, E. S.; Bukhtiyarov, P. G.; Palyanov, Y. N. Distribution of light alkanes in the reaction of graphite hydrogenation at pressure of 0.1-7.8GPa and temperatures of 1000-1350 degrees C. *High Pressure Research* **2018**, *38* (4), 468-481. DOI: 10.1080/08957959.2018.1517342.

(57) Syracuse, E. M.; van Keken, P. E.; Abers, G. A. The global range of subduction zone thermal models. *Physics of the Earth and Planetary Interiors* **2010**, *183* (1-2), 73-90. DOI: 10.1016/j.pepi.2010.02.004.